Available online at www.sciencedirect.com
ScienceDirect
International Journal of Solids and Structures 45 (2008) 1196–1216
INTERNATIONAL JOURNAL OF SOLIDS AND STRUCTURES
www.elsevier.com/locate/ijsolstr

Multi-mode wave propagation in ribbed plates. Part II: Predictions and comparisons

M.N. Ichchou *, J. Berthaut, M. Collet [1]

Laboratoire de Tribologie et Dynamique des Systèmes, École Centrale de Lyon-36, Avenue Guy de Collongues, 69130 Ecully, France

Received 15 February 2007; received in revised form 8 July 2007
Available online 11 September 2007

Abstract

This paper addresses dispersion curve numerical computations for specific ribbed plates. Precisely, wave propagation in the direction parallel to the ribs is the main objective. First, analytical calculations are performed for such ribbed plates after which the results are compared to a more general numerical procedure. This procedure reuses a reduced finite element model of the ribbed plate and extracts guided multi-mode propagation parameters. Comparisons of analytical and numerical estimations show very good agreement. Finally, the experimental results obtained in the companion paper are considered. Specifically, experimental and numerical dispersion curves are compared over a wide frequency range. Close concordance is obtained allowing the dispersion curves to be fully interpreted.

Keywords: Wave propagation; Bending vibration; Wave finite element; Medium frequencies; k-Space

1. Introduction

Analytical and numerical calculations of ribbed panel wavenumbers is the first objective of the present contribution. The second objective is to compare these predicted wavenumbers with the experimental results discussed in full in Part I of the paper (Ichchou et al., accepted for publication). This paper was also motivated by the analytical/numerical/experimental comparisons which are, at least to the authors point of view, a novel contribution to the field. Indeed, very few papers in the literature have dealt with the analytical calculation of ribbed panels up to now (Fahy and Lindqvist, 1976; Timoshenko, 1921; Timoshenko and Woinowski-Krieger, 1989; Cordonnier-Cloarec, 1989). The complexity of the analytical calculations involved has obliged authors to restrict their developments to simple ribbed panel configurations. Numerical computations of desired quantities is a relatively new and promising research subject (Finnveden, 1997; Gavric, 1994; Knothe et al., 1994; Finnveden, 1994; Orrenius and Finnveden, 1996). The ideas underlying such numerical developments are

* Corresponding author. Tel.: +33 04 72 18 62 30; fax: +33 04 72 18 91 44.
E-mail address: mohamed.ichchou@ec-lyon.fr (M.N. Ichchou).
[1] Also at: Institut FEMTO-ST, Laboratoire de Mécanique Appliquée R. Chaléat UMR 6174, Université de Franche-Comté-24, rue de l'Epitaphe, 25000 Besançon, France.

0020-7683/$ - see front matter
doi:10.1016/j.ijsolstr.2007.08.020

related to spectral finite element or to wave finite element techniques (Houillon et al., 2005; Mencik and Ichchou, 2005; Mace et al., 2005).

The analytical estimation of ribbed panel wavenumbers is strongly dependent on rib and panel geometries and on their coupling conditions. Furthermore, when focusing on flexural waves, analysis of how they propagate through such coupled structures requires simplification. Among these simplifications, the equivalent orthotropic plate theory (Timoshenko and Woinowski-Krieger, 1989; Cordonnier-Cloarec, 1989) (employed in the first part of this contribution (Ichchou et al., accepted for publication)) involves a basic propagation model and mechanism. It was shown in detail that the equivalent plate theory is only valid at low frequencies and in particular frequencies for which the wavelength is greater than the rib periodicity. Among further attempts to understand how flexural waves propagate in rib-stiffened plates, the work published by Fahy and Lindqvist (1976) is, in authors view, the most developed. This work addressed wave attenuation through complex rib-stiffened plates and proposed the complete analytical derivation of the dispersion curves for a beam/plate structure, taking into account the torsion/bending in the beam coupled with the plate bending. To achieve such an ''unwieldy'' derivation, several particular beam/plate geometries were considered. This paper takes the analysis provided in Fahy and Lindqvist (1976) a step further, in view to obtaining analytical/numerical/experimental ribbed panel dispersion curves for guided wave comparisons.

The ''unwieldiness'' of analytical development leads to a full numerical approach to propagation in complex structures. The main aim of most of these numerical methods is to take advantage of finite element modeling of a representative part of the structure. A finite element formulation is thus considered in the derivation of dispersion curves. Many authors have been interested in the numerical determination of dispersion curves for particular structures. Among them should be noted the work of Gavric (1994) and the contribution by Knothe et al. (1994). These authors applied this extraction technique to rail structures. Gavric (1994) proposed a particular finite element scheme allowing the extraction of wavenumbers from the resolution of a four order matrix equation. Knothe et al. (1994) introduced a numerical scheme well suited to infinite rail structures. The use of the latter allows dispersion curve extraction from a well-posed eigen-problem. Orrenius and Finnveden (1996) extended Gavric's work and applied it to rib-stiffened plates. Consequently, considering a span of the complex structure, a weak formulation was offered for the beam/plate system studied. Particular test functions are thus introduced in the formulation. These test functions present an exponential dependency along the propagation direction of the ribs with unknown wavenumbers. The finite element model obtained leads to the numerical estimation of guided wave dispersion curves. Finally Orrenius and Finnveden (1996) offered an interesting discussion on mode classification and categorization in rib-stiffened plates. Further analysis and newly published work of interest can be found in Benerjee and Kundu (2006a,b).

However, Gavric's approach runs into certain numerical difficulties. Indeed, the technique requires the development of a relatively new finite element code with specific elements, interpolation forms and an adapted eigenvalue extraction method. Some interesting alternative works on the problem at hand can be found in the literature on periodic structures and systems. Among these that by Lin (Lin and Donaldson, 1969) proposes in Lin and Donaldson (1969) a procedure using a transfer matrix concept in which beam-like structures as well as curved panel examples were examined. This method runs into difficulties due to the inversion of ill-conditioned matrices and the cumulative errors due to the transfer matrix assembly. Mead (1973, 1975) introduced fundamental and central ideas in the area of periodic system characterization. In this context, he proposed in Mead (1973) a quadratic and well-posed spectral problem in order to determine the wave propagation constants of a periodic system. This work was extended in Mead (1975). Mead (1975) proposed a second order matrix equation leading to the propagation constants of a periodic system. Tompson (1993) used the same technique after adding a damping contribution. Finally, mentioned should be made of the interesting work by Zhong and Williams (1995). Zhong (Zhong and Williams, 1995) offered a new eigenvalue problem, a kind of state space eigen-problem, wherein the main parameters are the displacement at both sections of the system considered. This approach was recently extended by Ichchou et al. (Houillon et al., 2005; Mencik and Ichchou, 2005) and by Mace (Mace et al., 2005), in which a number of applications are given for elastoacoustic and periodic structures and hollow structures. Here, the method is employed to deal with the numerical estimation of stiffened plate dispersion curves.

The objective of the present paper is twofold. Firstly, it is to compare analytical and numerical estimations of wave propagation parameters in rib-stiffened plate structures. The analytical developments are then offered

and commented in Section 2, whilst Section 3 summarizes the wave finite element technique devoted to dispersion curve estimation for complex periodic structures. The comparisons validate the analytical developments and confirm the generic nature of the numerical method implemented and employed here. The comparisons are described in Section 4. The second objective is to compare experimental and numerical wave propagation parameters. The comparisons are given in Section 5. Dispersion curves extracted from the developments of Part I (see Ichchou et al., accepted for publication) are shown to be in very good agreement with the numerical estimations. Both analytical/numerical and numerical/experimental comparisons are original insights into wave propagation in rib-stiffened plates, particularly in the context of multi-mode propagation mechanisms.

2. Analytical computations of ribbed plates wavenumbers

In this section, the analytical estimation of rib-stiffened plate wavenumbers is summarized. An in-depth analysis of this question was provided in the Fahy and Lindqvist (1976) paper. The paper (Fahy and Lindqvist, 1976) presents a number of beam/plate coupling cases and provides estimations of wave propagation parameters for several situations. In what follows, The analysis is restricted to the configuration shown in Fig. 1. It concerns a thin flexural vibrating finite plate (assumed to be isotropic and homogeneous). Shear and longitudinal waves are neglected through symmetry. The plate is coupled to two uniform beams representing the ribs. The beams and plate are assumed to be infinite in the direction of the ribs (x axis) as shown in Fig. 1. The ribs are assumed to be subjected to flexural as well as torsional motions.

The plate width is $2L$, infinite along the x axis. The beams are located, respectively, along edges $y = -L$ and $y = L$. The flexural motion of the plate is denoted w, the beam flexural motion is w_b and its torsional motion is denoted θ_b. Under Love–Kirchhoff assumptions, the flexural motion of the plate is governed by the following equation:

$$D\left(\frac{\partial^4 w}{\partial x^4} + 2\frac{\partial^4 w}{\partial x^2 \partial y^2} + \frac{\partial^4 w}{\partial y^4}\right) + \rho h \frac{\partial^2 w}{\partial t^2} = 0 \tag{1}$$

D being the plate flexural stiffness, ρ the mass density and h the thickness. The waveguide assumption along the x direction can be easily expressed as follows:

$$w = w_p e^{\alpha y} e^{i(\omega t - kx)} \tag{2}$$

the dispersion equation associated with wave propagating in the plate is thus:

$$\alpha^4 - 2\alpha^2 k^2 + k^4 - k_p^4 = 0 \tag{3}$$

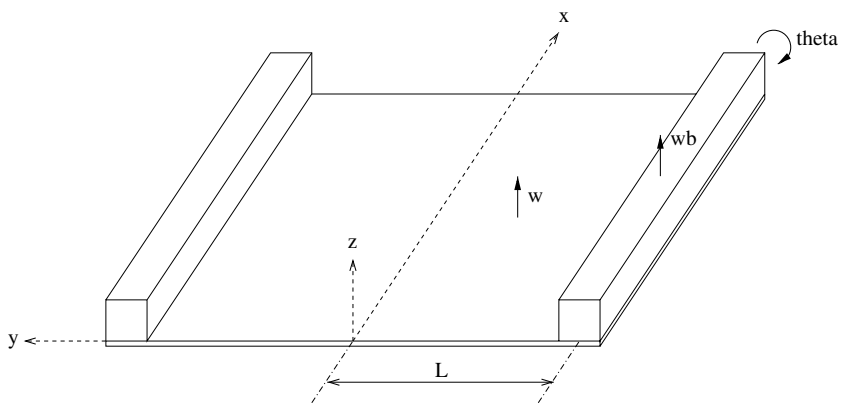

Fig. 1. Rib-stiffened plate geometry.

with $k_p^4 = \rho h\omega^2/D$, the uncoupled flexural wavenumber in the plate. This algebraic equation has four roots: λ_1 and $-\lambda_1$ with $\lambda_1^2 = k^2 + k_p^2$ and λ_2 and $-\lambda_2$ with $\lambda_2^2 = k_p^2 - k^2$, so that the free flexural behavior of the plate can be written as:

$$w(x,y,t) = \left(A^{(e)}\cosh\lambda_1 y + A^{(o)}\sinh\lambda_1 y + B^{(o)}\sin\lambda_2 y + B^{(e)}\cos\lambda_2 y\right)e^{\imath(\omega t - kx)} \tag{4}$$

where (e) and (o) designate even and odd, respectively, for convenience. Concerning the beam behavior, torsional and flexural motions are dealt with separately. Equations of motion are therefore the following:

$$EI\frac{\partial^4 w_b}{\partial x^4} + \rho S\frac{\partial^2 w_b}{\partial t^2} = D\left(\frac{\partial^3 w}{\partial y^3} + (2-\nu)\frac{\partial^3 w}{\partial x^2\,\partial y}\right)_{x=L^-} \tag{5}$$

$$GJ\frac{\partial^2 \theta_b}{\partial x^2} - \rho J\frac{\partial^2 \theta_b}{\partial t^2} = D\left(\frac{\partial^2 w}{\partial y^2} + \nu\frac{\partial^2 w}{\partial x^2}\right)_{x=L^-} \tag{6}$$

where I is the geometric inertia in relation to yy' axis, S the beam section and J the beam torsional inertia. The flexural and torsional solutions of the equations given can be readily expressed as follows:

$$w_b = \overline{w_b}\,e^{\imath(\omega t - kx)} \quad \text{and} \quad \theta_b = \overline{\theta_b}\,e^{\imath(\omega t - kx)} \tag{7}$$

At this stage it is more convenient to analyze symmetric and antisymmetric motional modes separately. Indeed, if symmetric motion is dealt with first, plate flexural behavior can be written as follows:

$$w(x,y,t) = (\cosh\lambda_1 y + \cos\lambda_2 y)e^{\imath(\omega t - kx)} \tag{8}$$

The beam/plate displacement continuity along $y = L$ leads to:

$$\overline{w_b} = A^{(e)}\cosh\lambda_1 L + B^{(e)}\cos\lambda_2 L \tag{9}$$

$$\overline{\theta_b} = A^{(e)}\lambda_1\sinh\lambda_1 L - B^{(e)}\lambda_2\sin\lambda_2 L \tag{10}$$

Using the following notations:

$$C_1 = \cosh\lambda_1 L \quad C_2 = \sinh\lambda_1 L$$
$$C_3 = \sin\lambda_2 L \quad C_4 = \cos\lambda_2 L$$

allows Eqs. (9) and (10) to be simply written as follows:

$$\overline{w_b} = A^{(e)}C_1 + B^{(e)}C_4$$
$$\overline{\theta_b} = A^{(e)}\lambda_1 C_2 - B^{(e)}\lambda_2 C_3$$

hence, through some analytical development Eqs. (5) and (6) leads to the expression:

$$A^{(e)}(C_1(k^4 - k_b^4) - \phi\lambda_1^3 C_2 + \phi(2-\nu)k^2\lambda_1 C_2) + B^{(e)}(C_4(k^4 - k_b^4) - \phi\lambda_2^3 C_3 - \phi(2-\nu)k^2\lambda_2 C_3) = 0 \tag{11}$$

$$A^{(e)}(\lambda_1 C_2(k^2 - k_T^2) + \tau\lambda_1^2 C_1 - \tau\nu k^2 C_1) + B^{(e)}(-\lambda_2 C_3(k^2 - k_T^2) - \tau\lambda_2^2 C_4 - \tau\nu k^2 C_4) = 0 \tag{12}$$

where the main parameters appearing in Eqs. (11) and (12) are the following: $k_b^4 = \rho S\omega^2/EI$, the beam uncoupled flexural wavenumber; $\phi = D/EI$, the flexural plate and beam stiffness ratio; $k_T^2 = \rho\omega^2/G$, the beam uncoupled torsional wavenumber; $\tau = D/GJ$, the flexural plate stiffness and torsional beam stiffness ratio. Eqs. (11) and (12) can be expressed in a standard algebraic format $\mathbb{T}.X = 0$ (where $X = [A^{(e)}\ B^{(e)}]$), whose singularization leads to the following dispersion equation:

$$\begin{aligned}&\lambda_2 C_1 C_3((k^4 - k_b^4)(k^2 - k_T^2) - \phi\tau(\lambda_1^2\lambda_2^2 + (2-\nu)k^2\lambda_1^2 - \lambda_2^2\nu k^2 - (2-\nu)\nu k^4)) + \lambda_1 C_2 C_4((k^4 - k_b^4)(k^2 - k_T^2)\\ &- \phi\tau(\lambda_1^2\lambda_2^2 - (2-\nu)k^2\lambda_2^2 + \lambda_1^2\nu k^2 - (2-\nu)\nu k^4)) + 2k_p^2\left(\tau C_1 C_4(k^4 - k_b^4) - \phi\lambda_1\lambda_2 C_2 C_3(k^2 - k_T^2)\right) = 0\end{aligned} \tag{13}$$

Eq. (13) gives the symmetric mode (beam/plate) coupled wavenumbers as a function of uncoupled plate flexural, beam flexural and beam torsional wavenumbers as well as geometrical constants, namely τ and ϕ. The numerical solution of Eq. (13) leads to the estimation of symmetric mode coupled wavenumbers for the beam/plate configuration given in Fig. 1.

Antisymmetric modes can also be represented through a similar analysis. Indeed, the plate flexural motion in this case becomes simply:

$$w(x,y,t) = (A^{(o)}\sinh\lambda_1 y + B^{(o)}\sin\lambda_2 y)e^{\imath(\omega t - kx)} \tag{14}$$

Along $y = L$ the beam/plate displacement continuity leads to the following expressions:

$$\overline{w_b} = A^{(o)}C_2 + B^{(o)}C_3 \tag{15}$$

$$\overline{\theta_b} = A^{(o)}\lambda_1 C_1 + B^{(o)}\lambda_2 C_4 \tag{16}$$

Eqs. (5) and (6) thus become:

$$A^{(o)}(C_2(k^4 - k_b^4) - \phi\lambda_1^3 C_1 + \phi(2-\nu)k^2\lambda_1 C_1) + B^{(o)}(C_3(k^4 - k_b^4) + \phi\lambda_2^3 C_4 + \phi(2-\nu)k^2\lambda_2 C_4) = 0 \tag{17}$$

$$A^{(o)}(\lambda_1 C_1(k^2 - k_T^2) + \tau\lambda_1^2 C_2 - \tau\nu k^2 C_2) + B^{(o)}(\lambda_2 C_4(k^2 - k_T^2) - \tau\lambda_2^2 C_3 - \tau\nu k^2 C_3) = 0 \tag{18}$$

Finally, the dispersion equation associated with the antisymmetric beam/plates coupled motion is given as follows:

$$\begin{aligned}&\lambda_1 C_1 C_3((k^4 - k_b^4)(k^2 - k_T^2) + \phi\tau(-\lambda_1^2\lambda_2^2 + (2-\nu)\nu k^4 + 2\lambda_2^2 k^2 - 2\nu k_p^2 k^2)) + \lambda_2 C_2 C_4(-(k^4 - k_b^4)(k^2 - k_T^2)\\ &+ \phi\tau(\lambda_1^2\lambda_2^2 - (2-\nu)\nu k^4 + 2\lambda_1^2 k^2 - 2\nu k_p^2 k^2)) + 2k_p^2(\tau C_2 C_3(k^4 - k_b^4) + \phi\lambda_1\lambda_2 C_1 C_4(k^2 - k_T^2)) = 0\end{aligned} \tag{19}$$

It should be noted that Eqs. (13) and (19) are first order polynomial versus ϕ and τ. Constant contributions are connected to the plate flexural motion. First order terms in ϕ are due to the beam and plate flexural coupling. First order terms in τ are due to the plate flexural and beam torsional coupling while first order terms in $\phi \times \tau$ are residual couplings between the beam flexural and torsional behaviors. These equations are solved in Section 4, where a comparison of analytical estimated wavenumbers and numerically computed wavenumbers are given. The numerical estimation of wavenumbers as general structural waveguides is commented in detail in the next section.

3. Wave finite element formulation (WFE)

As demonstrated in the previous section, the analytical calculations of wavenumbers are restricted to particular cases and often lead to very complex developments. Moreover, this type of analytical investigation is frequency dependent. High frequency behavior is in general very hard to represent in simple analytical theories. Indeed, high frequency behavior for the problem geometry considered in this paper is quit hard to solve analytically. The characterization of propagation constants of realistic guided structures with any cross-section is dealt with numerically in this section by using a novel numerical alternative. Initially, the finite element model of any cross-section topology of an elastic waveguide structure is used. When combined with an equivalent finite element model, the main guided propagation characteristic permits writing an eigenvalue problem. The numerical implementation of the resulting spectral problem in an FEM code allows the full numerical extraction of the guided dispersion curves. An application of the formulation to rib-stiffened plates is also provided in this section.

3.1. Formulation of an eigenvalue problem

The dynamics of straight elastic and dissipative structures is studied. A given straight structure is illustrated in Fig. 2: in the present framework, the system is assimilated with a set of identical subsystems connected along the main direction, let us say axis x, and whose left and right cross-sections (x-axis description) are denoted as `L` and `R`, respectively. The length of each subsystem along axis x is denoted as d. The formulation presented is based on the finite element model of a typical subsystem, as illustrated in Fig. 2, and whose kinematic variables, displacements and forces are written as $\mathbf{q}$ and $\mathbf{F}$, respectively. In what follows, mesh compatibility at the coupling interfaces between subsystems is assumed, implying that the left and right cross-sections of the considered subsystem contains the same number of degrees of freedom, i.e. n. The dynamical equilibrium equation of this subsystem at frequency $\omega/2\pi$, can be stated as follows (Zhong and Williams, 1995):

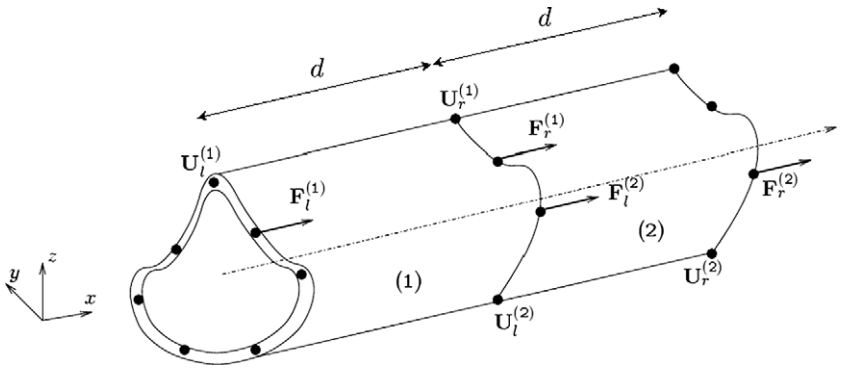

Fig. 2. Typical thin walled structure.

$$\begin{bmatrix} \mathbf{D}_{\mathrm{LL}} & \mathbf{D}_{\mathrm{LR}} \\ \mathbf{D}_{\mathrm{RL}} & \mathbf{D}_{\mathrm{RR}} \end{bmatrix} \begin{bmatrix} \mathbf{q}_{\mathrm{L}} \\ \mathbf{q}_{\mathrm{R}} \end{bmatrix} = \begin{bmatrix} \mathbf{F}_{\mathrm{L}} \\ \mathbf{F}_{\mathrm{R}} \end{bmatrix} \tag{20}$$

where $(n \times n)$ matrix $\mathbf{D}_{ij} = \mathbf{K}_{ij} - \omega^2\, \mathbf{M}_{ij}(\{i,j\} \in \{L,R\})$ stands for the ij component of the dynamic stiffness operator condensed on the left and right cross-sections, namely $\mathbf{D}$ (Zhong and Williams, 1995). Here, $\mathbf{K}$ and $\mathbf{M}$ stand for the stiffness and mass matrices, respectively. Dissipation can be considered through classical FEM models. According to Bloch's theorem (Broullouin, 1953), the dynamics of the global waveguide can be expanded on specific wave solutions with the form

$$\mathbf{q}_{\mathrm{R}} = \mu \mathbf{q}_{\mathrm{L}} \tag{21}$$

and

$$\mathbf{F}_{\mathrm{R}} = -\mu \mathbf{F}_{\mathrm{L}} \tag{22}$$

where μ denotes the propagation coefficient. Expressions (21) and (22) lead to an eigenvalue problem. Indeed, inserting Eqs. (21) and (22) into Eq. (20) leads to the following spectral problem (Houillon et al., 2005):

$$(\mathbf{D}_{\mathrm{RL}} + \mu_i(\mathbf{D}_{\mathrm{LL}} + \mathbf{D}_{\mathrm{RR}}) + \mu_i^2 \mathbf{D}_{\mathrm{LR}})(\mathbf{\Phi}_{\mathrm{q}})_i = 0 \tag{23}$$

where $\{(\mu_i, (\mathbf{\Phi}_{\mathrm{q}})_i)\}_{i=1,\ldots,2n}$ stands for the wave modes of the global system. A modified and well-conditioned format of the spectral problem can also be obtained. To achieve this, the use of a state vector representation is an interesting alternative to the spectral analysis which must be performed in the context of the numerical dispersion curve extraction (see Zhong and Williams, 1995 and Bocquillet et al., 2003 for detailed discussions). Indeed, given the following matrices:

$$\mathbf{S} = \begin{bmatrix} -\mathbf{D}_{\mathrm{LR}}^{-1}\mathbf{D}_{\mathrm{LL}} & -\mathbf{D}_{\mathrm{LR}}^{-1} \\ \mathbf{D}_{\mathrm{RL}} - \mathbf{D}_{\mathrm{RR}}\mathbf{D}_{\mathrm{LR}}^{-1}\mathbf{D}_{\mathrm{LL}} & -\mathbf{D}_{\mathrm{RR}}\mathbf{D}_{\mathrm{LR}}^{-1} \end{bmatrix} \tag{24}$$

and matrix $\mathbf{J}$, defined by:

$$\mathbf{J} = \begin{bmatrix} \mathbf{0} & \mathbf{I} \\ -\mathbf{I} & \mathbf{0} \end{bmatrix} \tag{25}$$

it can be readily shown that:

$$\mathbf{S}^T \mathbf{J} \mathbf{S} = \mathbf{J} \tag{26}$$

meaning that $\mathbf{S}$ is symplectic (Zhong and Williams, 1995). Ultimately, a spectral problem can be established as:

$$\mathbf{J}\mathbf{\Phi}_i = \mu_i \mathbf{S}^T \mathbf{J}\mathbf{\Phi}_i \tag{27}$$

which leads to

$$\mathbf{J}^{-1}\mathbf{S}^{-T}\mathbf{J}\mathbf{\Phi}_i = \mu_i\mathbf{\Phi}_i \tag{28}$$

and thus, considering that matrix $\mathbf{S}$ is symplectic ($\mathbf{S}^{-T} = \mathbf{J}\mathbf{S}\mathbf{J}^{-1}$ (Zhong and Williams, 1995)),

$$\mathbf{S}\mathbf{\Phi}_i = \mu_i\mathbf{\Phi}_i \tag{29}$$

Here $\mathbf{\Phi}_i = ((\mathbf{\Phi}_{\mathrm{q}})_i^T(\mathbf{\Phi}_{\mathrm{F}})_i^T)^T$ stands for the ith eigenvector of operator $\mathbf{S}$, which is broken down into $(n\times 1)$ displacements $\mathbf{q}$ and force $\mathbf{F}$ wave components. The frequency response of the global system can be expressed by expanding the kinematic variables of the considered subsystem on the basis of eigenvectors:

$$\begin{pmatrix}\mathbf{q}_{\mathrm{L}}\\ -\mathbf{F}_{\mathrm{L}}\end{pmatrix} = \begin{bmatrix}\mathbf{\Phi}_{\mathrm{q}}\\ \mathbf{\Phi}_{\mathrm{F}}\end{bmatrix}\mathbf{Q}_{\mathrm{L}} \quad \text{and} \quad \begin{pmatrix}\mathbf{q}_{\mathrm{R}}\\ \mathbf{F}_{\mathrm{R}}\end{pmatrix} = \begin{bmatrix}\mathbf{\Phi}_{\mathrm{q}}\\ \mathbf{\Phi}_{\mathrm{F}}\end{bmatrix}\mathbf{Q}_{\mathrm{R}} \tag{30}$$

where $\mathbf{\Phi}_{\mathrm{q}}$ and $\mathbf{\Phi}_{\mathrm{F}}$ stand for the matrices of eigenvector $\{(\mathbf{\Phi}_{\mathrm{q}})_i\}_i$ and $\{(\mathbf{\Phi}_{\mathrm{F}})_i\}_i$, respectively (Mencik and Ichchou, 2007), and where $\mathbf{Q}_{\mathrm{L}}$ and $\mathbf{Q}_{\mathrm{R}}$ stand for the $(2n\times 1)$ generalized coordinates evaluated for the left and right boundaries of the subsystem, respectively. It has been shown in Yong and Lin (1989) and Mencik and Ichchou (2007) that generalized coordinates $\mathbf{Q}_{\mathrm{L}}$ and $\mathbf{Q}_{\mathrm{R}}$ can be related in this way

$$\mathbf{Q}_{\mathrm{R}} = \begin{bmatrix}\mu & \mathbf{0}\\ \mathbf{0} & \mu^{-1}\end{bmatrix}\mathbf{Q}_{\mathrm{L}} \tag{31}$$

where $\boldsymbol{\mu}$ stands for the matrix of eigenvalues $\{\boldsymbol{\mu}_i\}_{i=1,\ldots,n}$. Note that the description provided by Eq. (31) is based on the classification of the eigenvectors into incident and reflected waves. Further developments and details concerning this method are presented in Mencik and Ichchou (2005, 2007).

3.2. Ribbed panel case study: general considerations

The approach explained previously will be employed here in the rib-stiffened plate case. Fig. 3 shows the finite element modeling of the beam/plate structure. A restricted finite element part is used for computing wavenumbers as indicated in Fig. 4. A 2D finite element model was established to reduce the computation cost. The plate is modeled with 21 thin plate elements with thickness h. A dynamic condensation was achieved using 2 nodal degrees of freedom (displacement w along z axis, rotation rot_x in the (y,z) plane). The rib is modeled with a thin plate element with a thickness b and $\frac{b+h}{2}$ shifted along the z axis with rigid massless elements.

To complete the analysis, the question of boundary conditions in the model shown in Fig. 4, namely for $y = 0$ and $y = p$, should be discussed. Strictly speaking, these boundaries conditions should represent periodic behavior, the employed numerical part shown in Fig. 4 being a "sample" of the structure represented in Fig. 3. Moreover, the numerical approach should represent, at least along the x axis, a very large number of possible

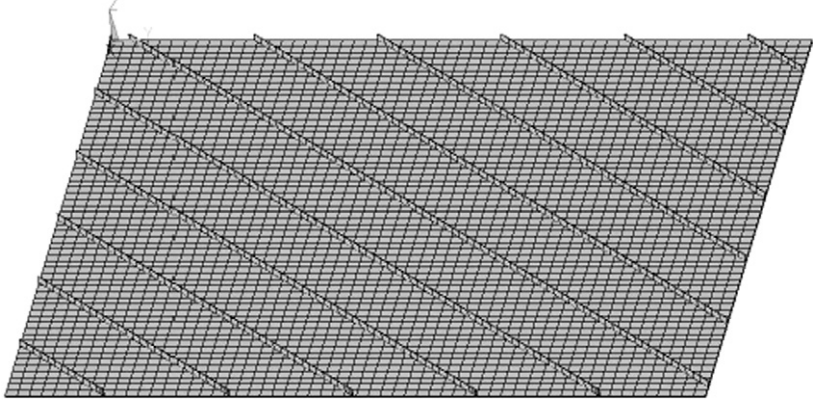

Fig. 3. FEM model of the rib-stiffened plate.

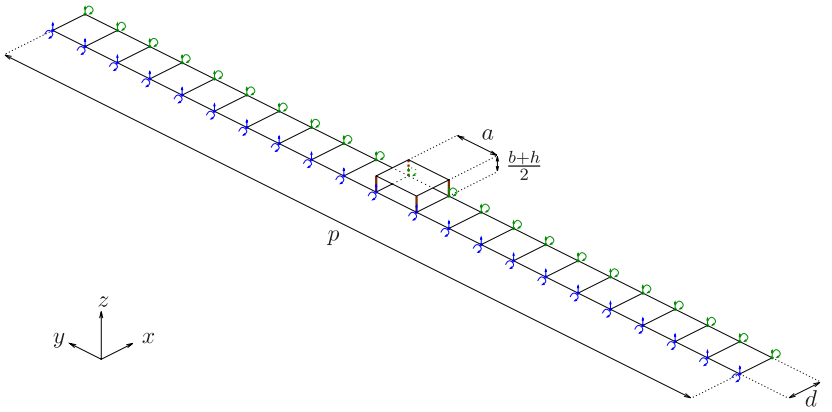

Fig. 4. Rib-stiffened plate FEM used for the extraction of guided wavenumbers.

guided motions. Therefore the coupled conditions constitute one of the possible boundary conditions to be employed, namely:

$$\begin{cases} w|_{y=0} = w|_{y=p} \\ \mathrm{rot}_x|_{y=0} = \mathrm{rot}_x|_{y=p} \end{cases} \tag{32}$$

These boundaries, defined by CP below, couple flexural and rotational motion at the sample (see Fig. 4) boundaries and simulate a periodic situation. Such boundaries allow a definition of the deformed plane wave shape (Fig. 5 – mode 0) and the first guided bending mode (Fig. 5 – mode 1). The next mode predicted is drawn in Fig. 6. For this deformed shape, the boundary conditions are respected and two vibration lobes are predicted. The motion of the main rib is expected to be torsional, hence this mode is denoted $2^{(T)}$. However, at low frequencies, with torsional rigidity much higher than flexural rigidity, the flexural motion of the ribs is predicted rather easily (see Fig. 6). The boundary conditions at the sample boundaries are thus simple supports (SS in the following) as clearly shown in Fig. 6. Thus, considering pure SS boundary conditions, some predicted deformed mode shapes are given in Fig. 7. The first mode under such boundary conditions (Fig. 7, left given sketch), has two flexural lobes and seems to involve the rib bending motion. The mode $2^{(T)}$ already described (using CP conditions) is found. Thus, it seems that a combination between CP and SS boundary conditions is needed to extract all the predicted deformed shapes. More precisely, modes 0 and 1 are obtained thanks to CP conditions, whilst the second mode requires SS boundaries. Following this analysis, the predicted higher order deformed shapes are drawn in Fig. 8 where CP boundary conditions are employed, and Fig. 9 shows SS boundary results. The analysis of Figs. 8 and 9 confirms the relevance of the conclusions for lower mode extraction. Indeed, the CP boundary conditions show an odd flexural mode and then an even torsional mode while the SS boundary conditions show an even flexural mode and then an odd torsional motion.

3.3. Ribbed panel case study: numerical analysis

The previous subsection established the boundary conditions to be used in order to fully describe the flexural behavior of the rib-stiffened plate and illustrated that two boundary condition configurations are needed

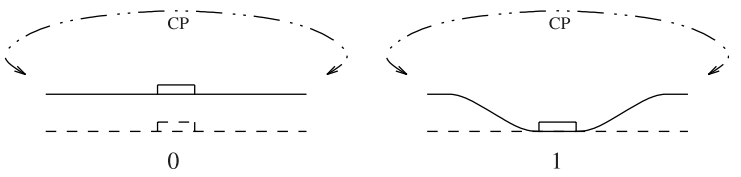

Fig. 5. Sketch of predicted deformed shapes: mode 0 (rigid mode) and mode 1 (first flexural mode).

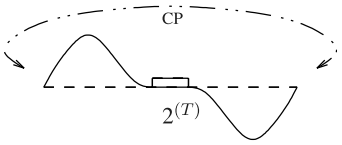

Fig. 6. Sketch of the next predicted mode with CP boundary conditions.

Fig. 7. Sketch of first deformed shapes with SS boundaries.

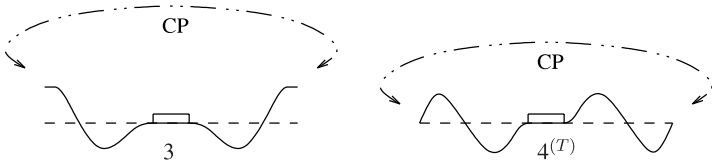

Fig. 8. Sketch of CP higher order modes.

Fig. 9. Sketch of SS higher order modes.

to achieve this goal. Consequently, considering the rib-stiffened plate shown in Figs. 3 and 4, the spectral problem formulated in Eq. (29) was treated numerically over a wide frequency range (from 0 to 6400 Hz) in both cases. Fig. 10, shows the results (given in terms of the $\omega \rightarrow k_{\omega}^{(i)}$ function, guided wave dispersion curves). Moreover, the WFE allows deformed mode shapes to be drawn numerically. These deformed shapes are simply eigenvectors of the formulation established above (Eq. (29)).

With the CP boundary conditions, the propagation branch denoted 1, in Fig. 10 has a rigid deformed shape at 0 Hz (the plane wave) and a deformed shape corresponding to that predicted (see Fig. 5) at 6400 Hz. The plot of the numerical eigenvectors obtained by the numerical simulation in Fig. 10 fully confirms this analysis. At higher frequencies this mode follows a $Dk^4 = \rho h \omega^2$ propagation law. The second propagation branch under the same boundary conditions (branch 2 in the CP calculations) corresponds to the branch denoted branch 6 in the SS computations. This branch is thus the $2^{(T)}$ torsional mode shown previously. Moreover, the result shown in Fig. 11 (SS boundary conditions) shows that the $2^{(T)}$ branch converges toward branch 7. The latter represents mode 2 and the convergence is easy to understand. Similar comments can be drawn for the other propagation branches appearing in Fig. 11. For instance, in the CP calculation, propagation branch 3 corresponds to mode 3 defined previously, and only appears for such boundary conditions. The next propagation branch (number 4) is another flexural mode and also appears in the SS computation (branch 8). For the sake of clarity, the following figures summarize the obtained results and focus on deformed shape definition. Fig. 12 plots the deformed shape corresponding to branch 1. This result is in perfect accordance with that provided in Fig. 5. Fig. 13 represents the deformed shape corresponding to branch 2 (in CP calculations) and to branch 6 (in SS calculations). This result is to be compared with that predicted in Fig. 7 – 2 (left). Fig. 14, illustrates the first torsion mode. The rib section rotates due to system torsion close to the cut-on frequency (1020 Hz). At a higher frequency (6400 Hz) the torsion is no longer visible. It should be pointed out that this result corresponds perfectly to the predicted result given in Figs. 6 and 7 – $2^{(T)}$. Fig. 15 plots mode 3, from its cut-on frequency (985 Hz) and at higher frequencies (6400 Hz). This mode perfectly agrees with that shown in Fig. 8 – 3. Finally, Fig. 16 shows mode 4 from its cut-on frequency 2285 Hz and at a higher fre-

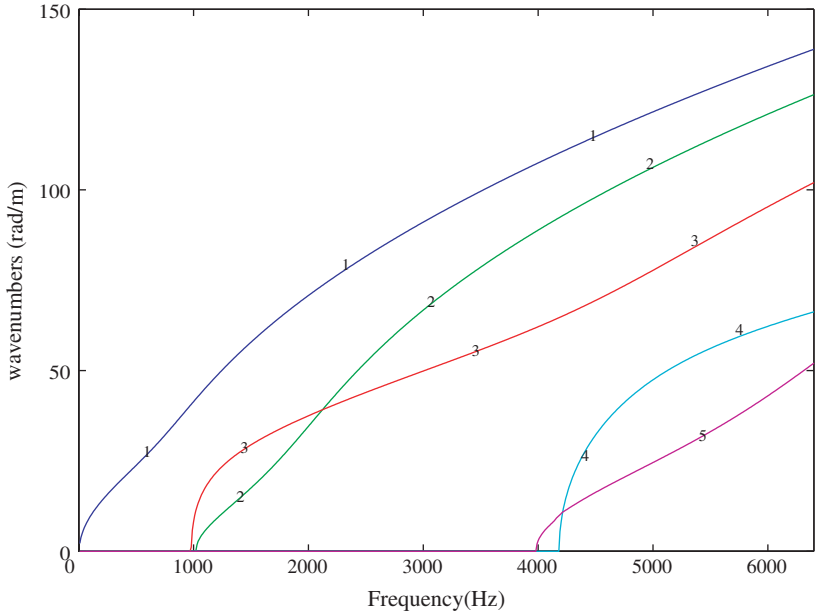

Fig. 10. WFE guided wavenumbers prediction for the rib-stiffened plate: CP boundary conditions.

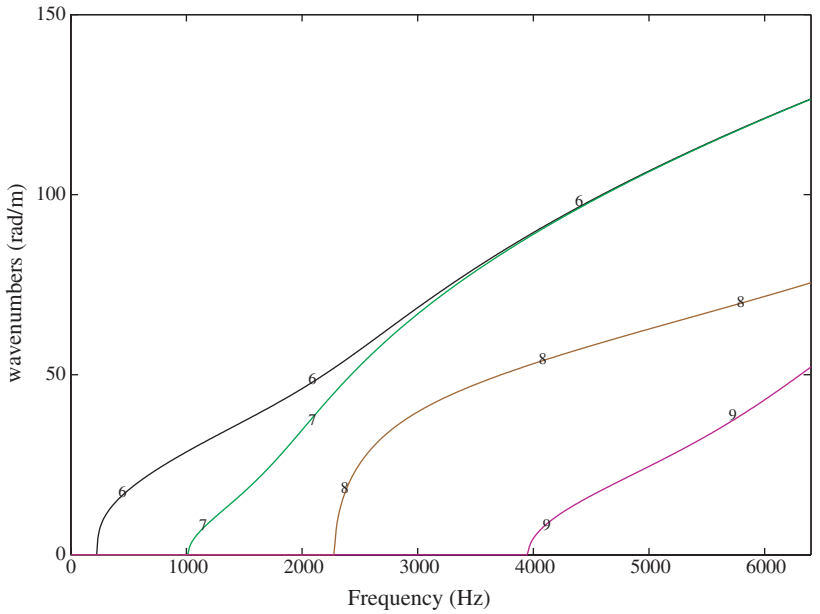

Fig. 11. WFE guided wavenumbers prediction for the rib-stiffened plate: SS boundary conditions.

quency (6400 Hz). This eigenvector corresponds to the one plotted in Fig. 9 – 4. On the basis of the analysis provided in this section, a numerical alternative capable of predicting guided waves was proposed. The formulation is general and generic. Its implementation in a finite element environment allows it to be used for very complex waveguides. In this section, the numerical formulation was applied to the rib-stiffened plate case study. The results obtained seem to be in good agreement with the predicted physical behavior. In the next section, the formulation results are compared in detail to the analytical estimation of wavenumbers given

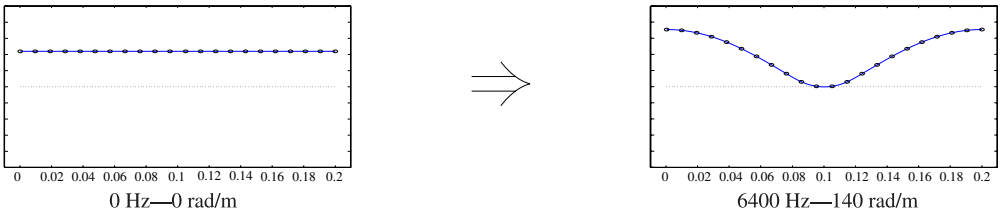

Fig. 12. Deformed shape corresponding to branch 1 at 0 Hz and 6400 Hz.

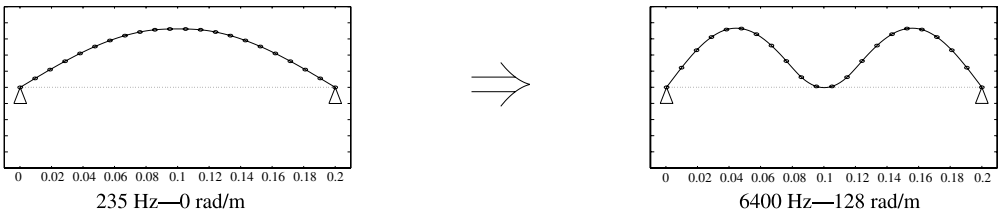

Fig. 13. Deformed shape corresponding to branch 2 and to branch 6 at 0 Hz and 6400 Hz.

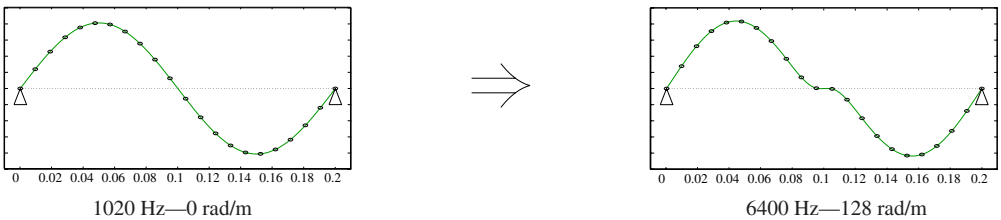

Fig. 14. Torsion deformed shape (2 lobes) at the cut-on frequency and at a higher frequency.

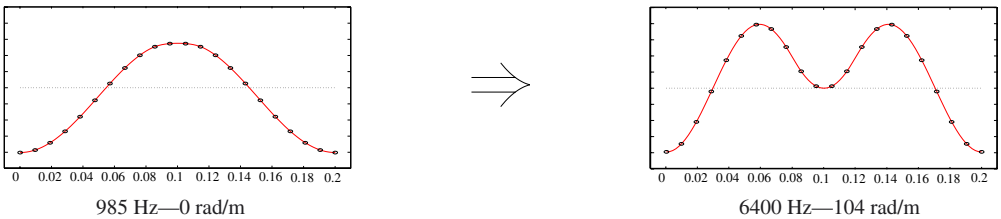

Fig. 15. Deformed shape of the third flexural mode at the cut-on frequency and at a higher frequency.

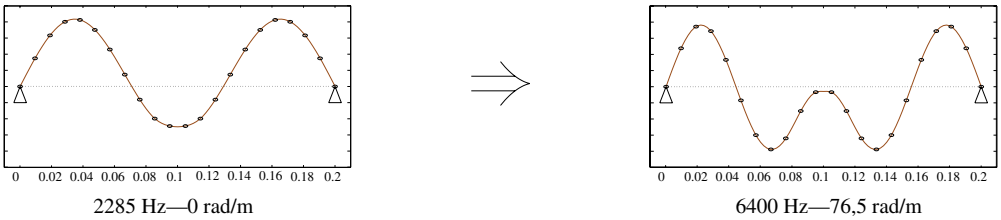

Fig. 16. Deformed shape of the fourth flexural mode at the cut-on frequency and at a higher frequency.

in Section 2. A final comparison will be performed with the experimental results derived from the companion paper (Ichchou et al., accepted for publication).

4. Analytical and WFE comparisons

The aim of this section is to compare the analytical formulation (specifically Eqs. (13) and (19)) with the numerical formulation (Eq. (29)) for several cases. Table 1 provides data needed and inputs for both formulations. A parametric survey is also carried. Three rib spacings are thus considered in the comparisons ($p = 40$ cm, $p = 20$ cm and $p = 10$ cm are, respectively, tested). The parameters needed for Eqs. (13) and (19) are thus the following: $D = 13.7$ Nm, $S = 6.25 \times 10^{-5}$ m^2, $I = 2.03 \times 10^{-10}$ m^4, $J = 7.24 \times 10^{-10}$ m^4. Thus, detailed parameters in the analytical model can be estimated as follows: $k_p = 0.711\sqrt{\omega}$, $k_b = 0.327\sqrt{\omega}$, $k_T = 3.15 \times 10^{-4}\omega$, $\phi = 0.898$ m^{-1}, $\tau = 0.671$ m^{-1}. Parameter L is defined as the distance between the system symmetry axis and the neutral axis of the beam (Fahy and Lindqvist, 1976). In the calculations done later, the L definition is slightly different, as shown in Fig. 17. This definition leads to $L = \frac{p-a}{2}$. Thus L is, respectively, equal to 0.195 m, 0.095 m and 0.045 m for the three cases considered (see Figs. 18 and 19). Comparisons between calculations of numerical and analytical propagation constants are presented in Fig. 20. Solid line results are the analytical estimation of wavenumbers (symmetric and antisymmetric modes) obtained by resolving Eqs. (13) and (19). Dotted line branches are the uncoupled wavenumbers: beam torsional wavenumber (the straight line $k_T \propto \omega$), the beam flexural wavenumber (parabola $k_b \propto \sqrt{\omega}$) and the plate flexural wavenumbers (parabola $k_p \propto \sqrt{\omega}$). The dotted lines in Fig. 20 are the results of the wave finite element calculations.

The predicted analytical branches (see Fig. 21) present two main stages that demarcate three different zones. These stages appear when the dispersion equation corresponding to a given branch approaches the uncoupled dispersion equation (beam torsional and flexural motions). Thus in the first zone the torsional motion of the beam dominates the behavior. In the second, the beam flexural motion is the dominating mechanism, whilst the plate flexural motion dominates the last delimited zone (the ribs are almost motionless) (see Fig. 21). The comparisons between the predicted numerical (dashed lines) and the analytical (solid lines) wavenumbers show good agreement, particularly for the beam and plate flexural zones (zones 2 and 3 in Fig. 21). The estimated numerical parameters show only one visible stage corresponding to the beam flexural dispersion equation. Such observations are persistent for the three different cases studied. Another set of computations was conducted in which the beam torsional motion was canceled. Hence, setting $\tau = 0$ in Eqs. (13) and (19) leads to the following simplified formats:

$$\left(\frac{C_4}{C_3\lambda_2} + \frac{C_1}{C_2\lambda_1}\right)(k^4 - k_b^4) - 2k_p^2\phi = 0 \tag{33}$$

$$\left(\frac{C_3}{C_4\lambda_2} - \frac{C_2}{C_1\lambda_1}\right)(k^4 - k_b^4) + 2k_p^2\phi = 0 \tag{34}$$

Figs. 22–24 show the numerical and analytical comparisons when the beam torsion was canceled from the analytical calculations. The comparisons show better tendencies. The deviation between numerical and analytical estimations is relatively weak and mainly concentrated in the beam domination zone, where the analytical approach slightly over-estimate the wavenumbers. Hence, globally convincing agreements were shown in the numerical and analytical comparisons. Of course, it should be noted that the analytical computations are lim-

Table 1
Plate and ribs characteristics

ρ	E	v	G	h
Plate				
2800 kg m^{-3}	75 GPa	0.33	28 GPa	1.25 mm

ρ	E	v	G	a	b
Ribs					
2800 kg m^{-3}	75 GPa	0.33	28 GPa	10 mm	5 mm

Case A	Case B	Case C
Spacings		
$p = 40$ cm	$p = 20$ cm	$p = 10$ cm

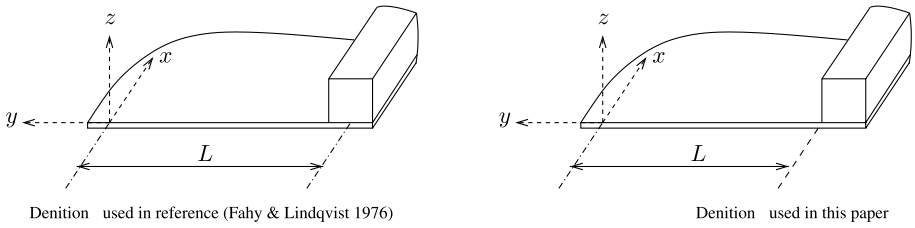

Fig. 17. The parameter L definition.

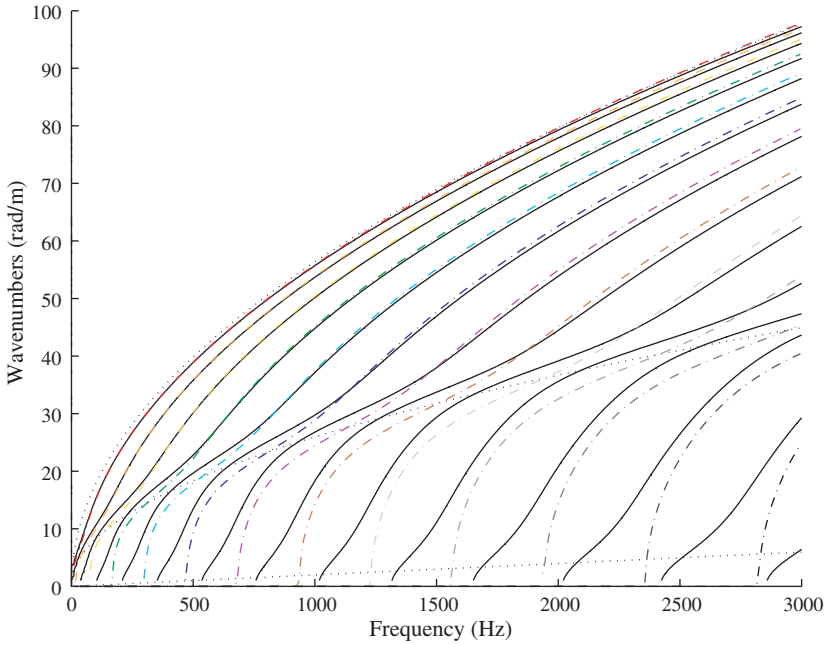

Fig. 18. Dispersion curves comparisons – case A: (solid line) analytical predictions, (dashed lines) WFEM numerical predictions, (doted lines) ribs torsional, ribs flexural and plate flexural uncoupled wavenumbers.

ited to simple geometries whilst the numerical computations are conceivable for a wide range of applications. In the next section the numerical computations will finally be compared to experimental results.

5. Experimental/numerical validations

In this section the experimental results obtained and discussed in the companion paper (Ichchou et al., submitted for publication) are compared to numerical estimations of wavenumbers obtained by the WFE formulation (see Eq. (29)). A two step comparison strategy was employed. The first step consisted in comparing the numerical extracted guided dominant wavenumbers with the experiments. The latter was obtained by the IWC algorithm described in the companion paper (see Ichchou et al., accepted for publication). The second step, consisted in a full comparison of the identified numerical and experimental dispersion curves associated with the multi-mode propagation behavior of the ribbed stiffened plates.

5.1. Dominants wavenumbers comparisons

In the first step of the comparison, the dominant wavenumbers were extracted. The question relating to their estimation is quite simple. It consists in the characterization of the propagation parameters along the

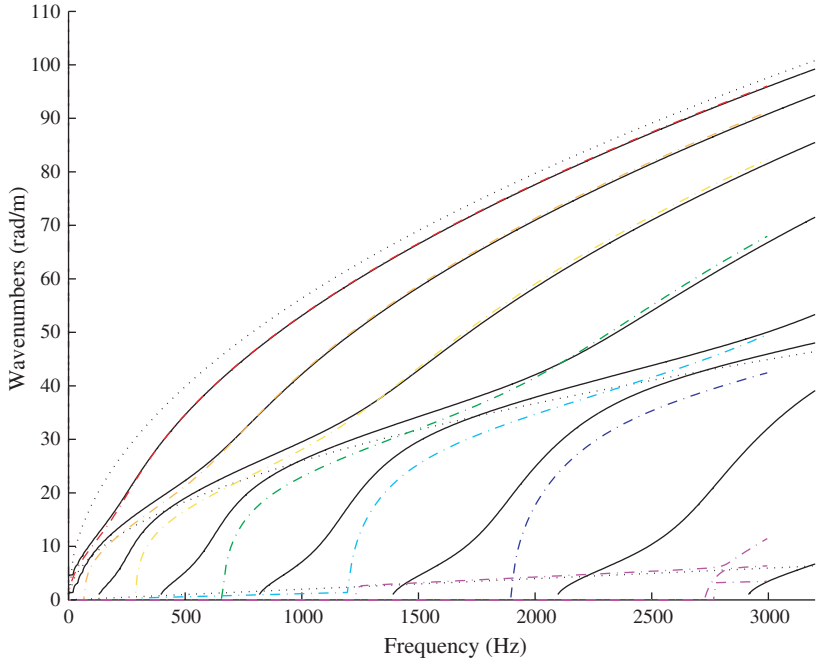

Fig. 19. Dispersion curves comparisons – case B: (solid line) analytical predictions, (dashed lines) WFEM numerical predictions, (dotted lines) ribs torsional, ribs flexural and plate flexural uncoupled wavenumbers.

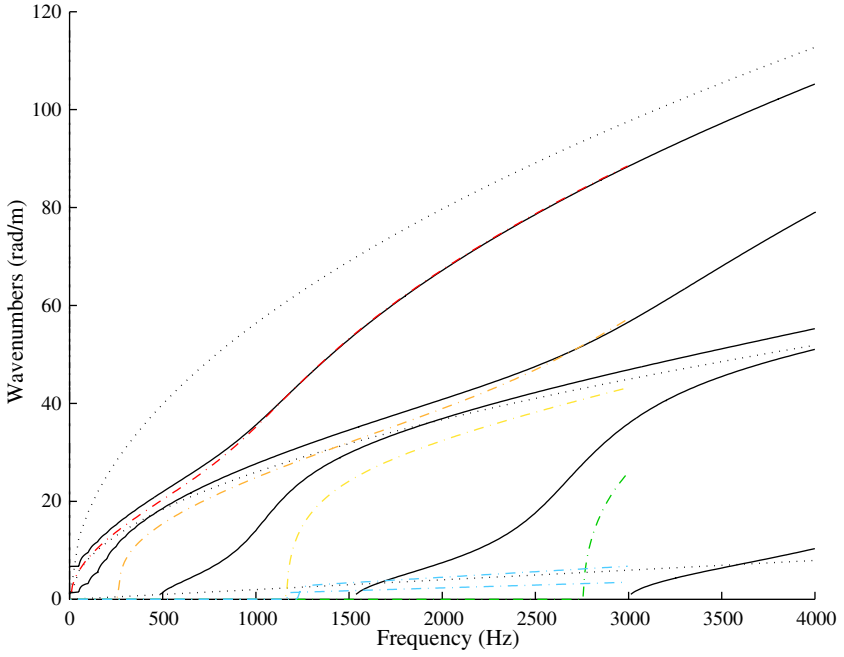

Fig. 20. Dispersion curves comparisons – case C: (solid line) analytical predictions, (dashed lines) WFEM numerical predictions, (doted lines) ribs torsional, ribs flexural and plate flexural uncoupled wavenumbers.

main directions, precisely x' (rib direction) and y' (directions orthogonal to the ribs). To obtain such properties, the IWC method described in the companion paper (Ichchou et al., accepted for publication), was used only for wave headings $(\theta_\perp + i\frac{\pi}{2})_{i\in[[-1\ldots2]]}$. The orthotropic nature of the field involves a symmetry related to

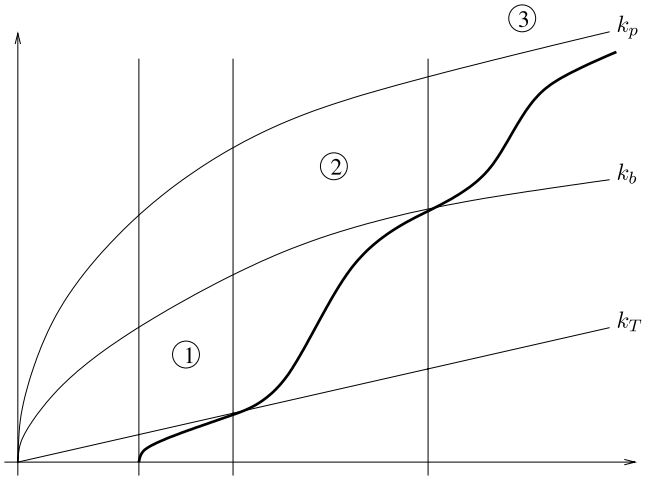

Fig. 21. Sketch of the analytical mode behavior.

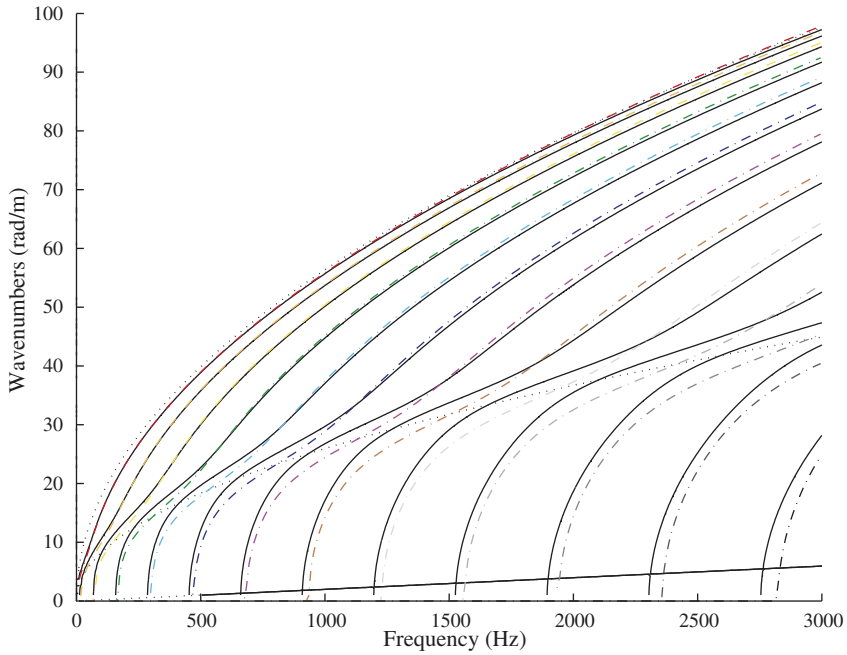

Fig. 22. Dispersion curves comparisons with torsion coupling canceled in the analytical estimations – case A: (solid line) analytical predictions, (dashed lines) WFEM numerical predictions, (doted lines) rib torsional, rib flexural and plate flexural uncoupled wavenumbers.

the principal directions x' and y'. Consequently, wavenumbers such that $(\theta_\perp, \theta_\perp + \pi)$ (representing $k_{x'}$ and $-k_{x'}$) and wavenumbers $(\theta_\perp + \frac{\pi}{2}, \theta_\perp - \frac{\pi}{2})$ are grouped, respectively. Fig. 25 presents the IWC results for these restricted directions. This figure shows the $k_{x'}$ and $k_{y'}$ results. Moreover, the structural orthotropy parabola ($k_{x'} = \widetilde{D}_{x'}^{-1/4}\sqrt{\omega}$ and $k_{y'} = \widetilde{D}_{y'}^{-1/4}\sqrt{\omega}$) are added to the figure ($\widetilde{D}_{x'}$ and $\widetilde{D}_{y'}$ being the equivalent stiffnesses calculated in part I of this contribution (Ichchou et al., accepted for publication)). The first flexural mode (see Fig. 10) numerically estimated by the WFE approach is also shown (with CP boundary conditions) in this figure. Fig. 25 therefore shows very good agreement between the estimated and experimental results. Figs. 27 and 26 concern cases B and C, respectively (with 20 cm and 10 cm rib spacings). Although the global tendencies are respected, the comparisons are less convincing.

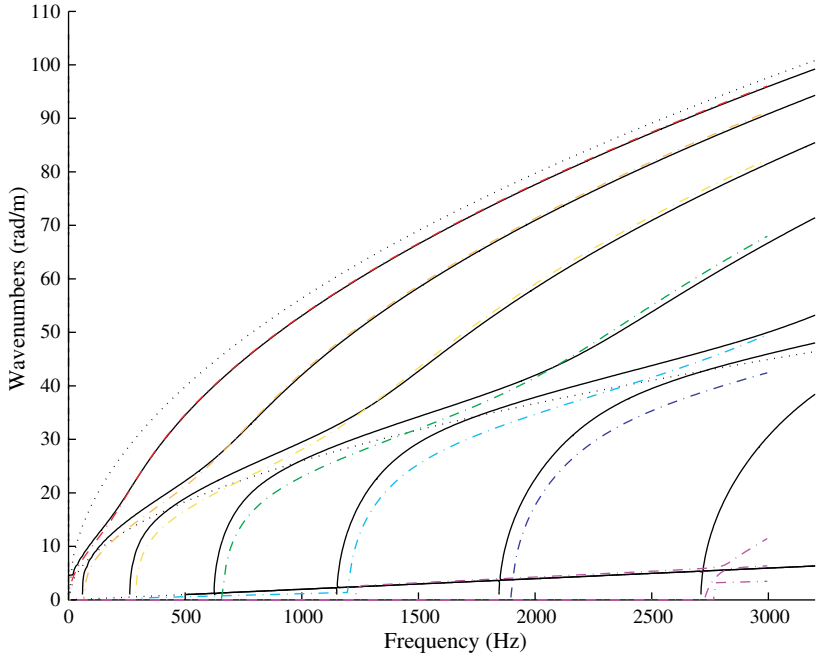

Fig. 23. Dispersion curves comparisons with torsion coupling canceled in the analytical estimations – case B: (solid line) analytical predictions, (dashed lines) WFEM numerical predictions, (doted lines) ribs torsional, ribs flexural and plate flexural uncoupled wavenumbers.

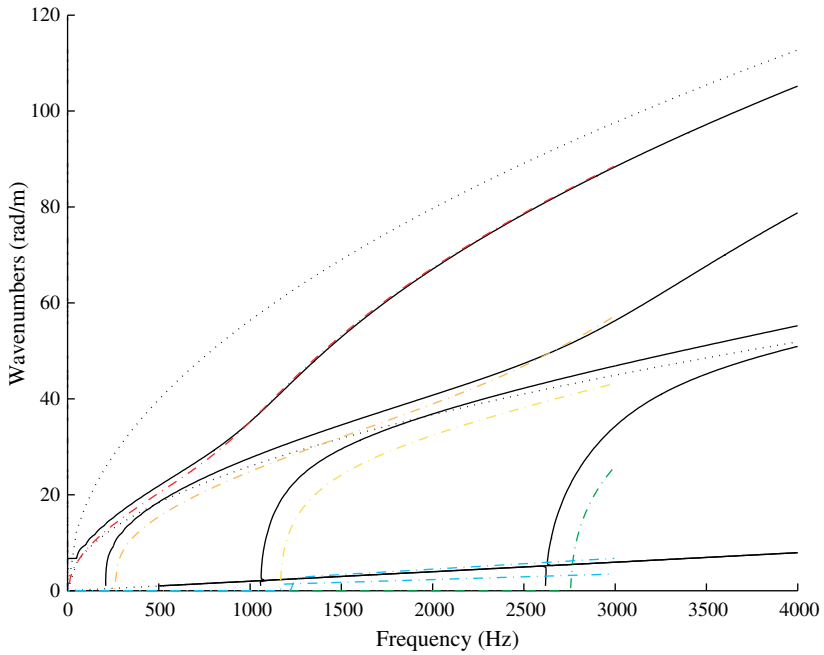

Fig. 24. Dispersion curves comparisons with torsion coupling canceled in the analytical estimations – case C: (solid line) analytical predictions, (dashed lines) WFEM numerical predictions, (doted lines) ribs torsional, ribs flexural and plate flexural uncoupled wavenumbers.

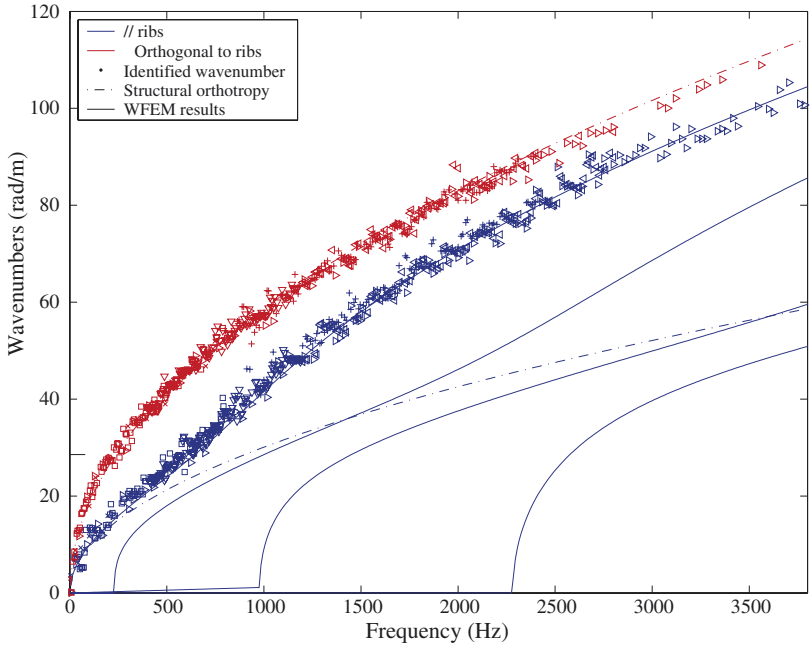

Fig. 25. Frequency dependent dominant wavenumbers for the two orthotropy direction x' and y' – case A: '+', 'o', ◁ experimental results.

5.2. Multi-mode propagation branches comparisons

Figs. 28–30 show comparisons between numerical estimations of guided wave parameters and experimental results obtained in the companion paper. The concordance between both predicted and experimental values is quite good and verified for the three experimental set-ups used and given in Table 1.

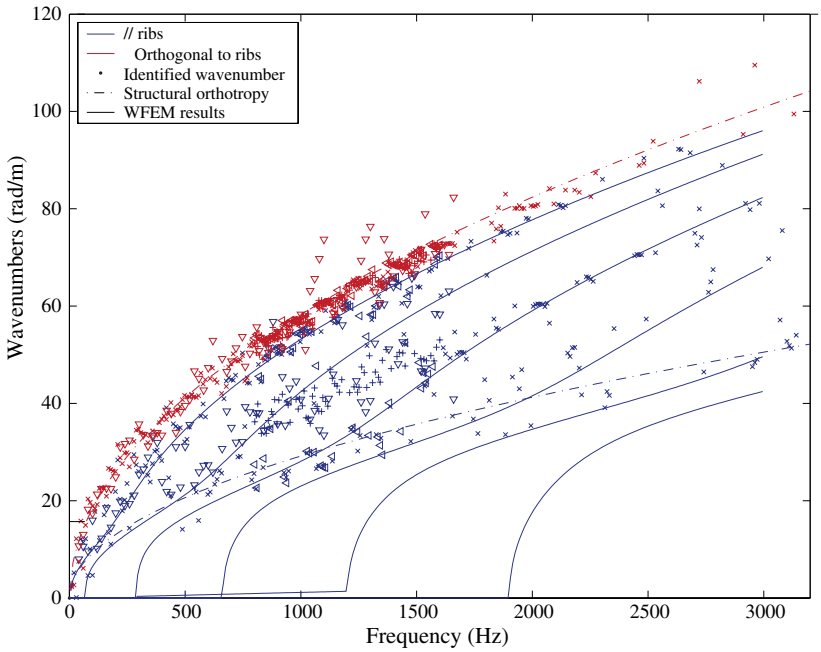

Fig. 26. Frequency dependent dominant wavenumbers for the two orthotropy direction x' and y' – case B: ★, ◁ experimental results.

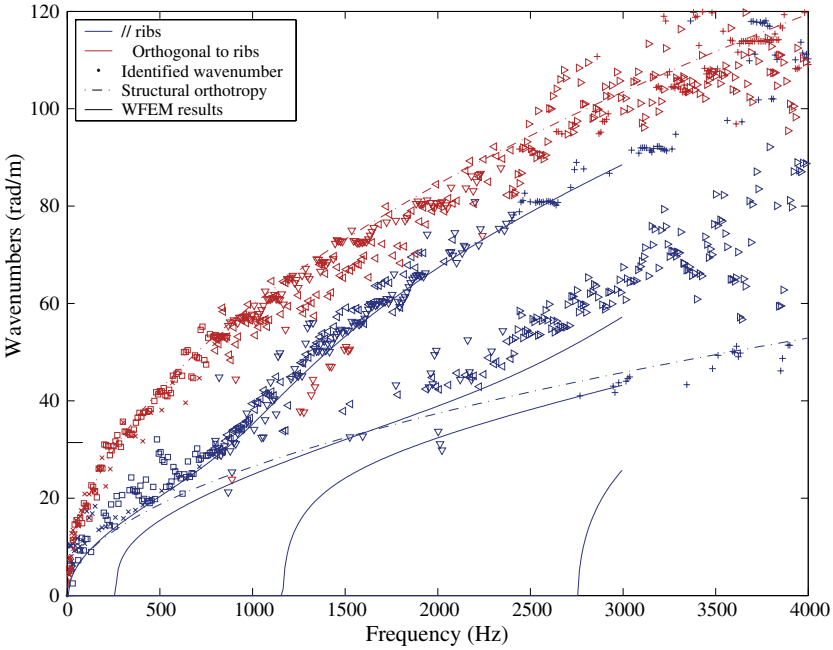

Fig. 27. Frequency dependent dominant wavenumbers for the two orthotropy direction x' and y' – case C: ◁ experimental results.

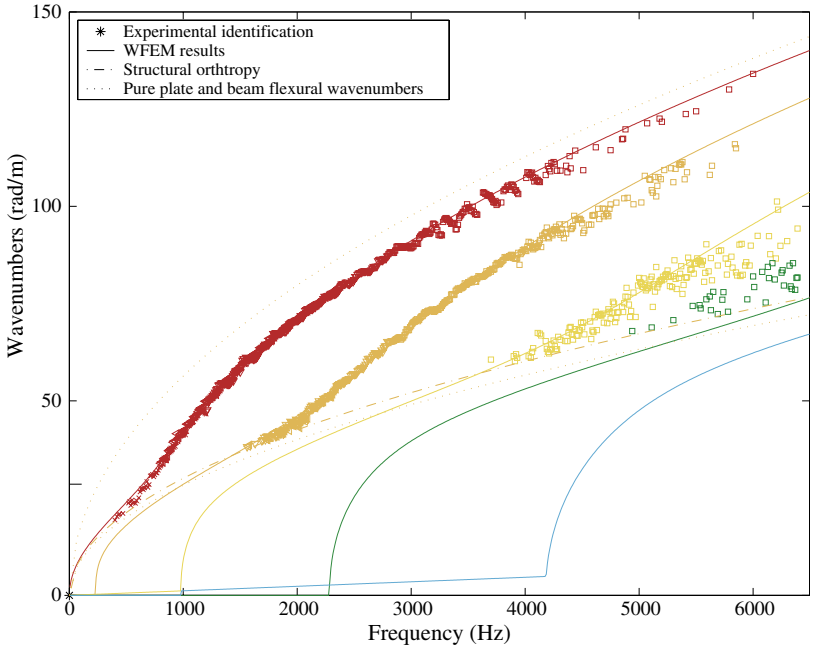

Fig. 28. Frequency dependent multi-mode propagation branches – case A: ◁ experimental results.

6. Concluding remarks

This paper addressed the estimation of guided wave characteristics with emphasis given to the analysis of wave propagation in rib-stiffened plates. Analytical, numerical and experimental characterizations of flexural waves in such structures were presented and the main results can be summarized as follows:

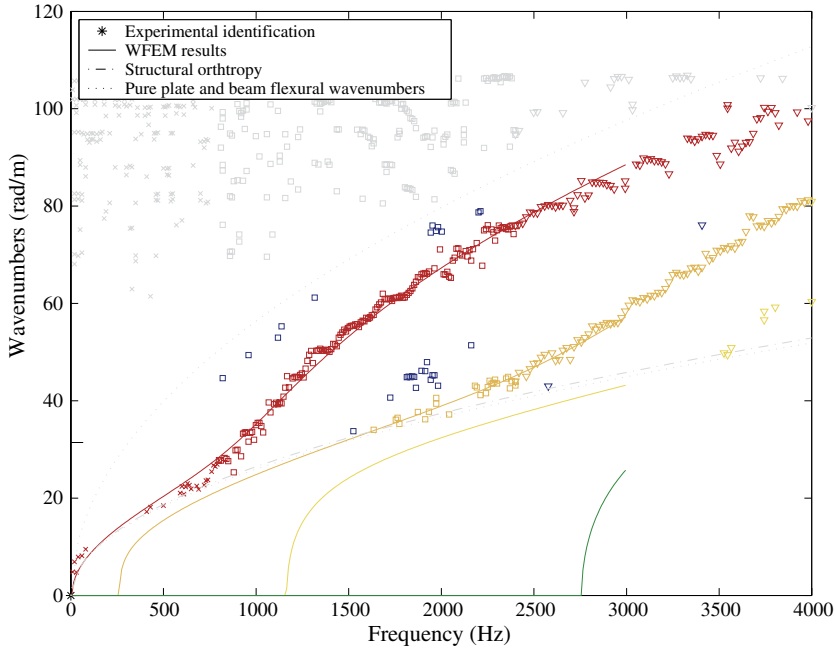

Fig. 29. Frequency dependent multi-mode propagation branches – case B: ◁ experimental results.

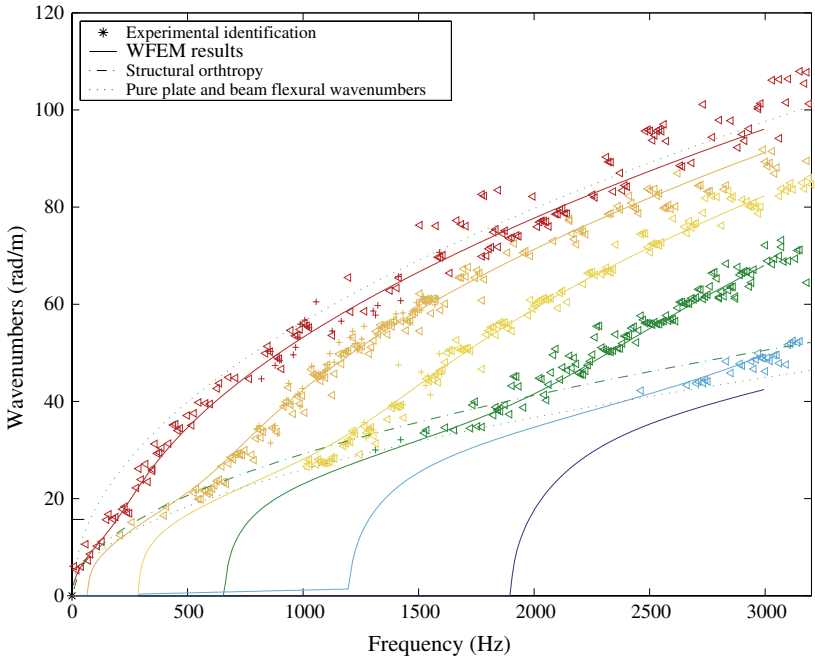

Fig. 30. Frequency dependent multi-mode propagation branches – case C: ◁ experimental results.

– Analytical estimations of wave propagation parameters were performed for the rib-stiffened plate considered. This analytical calculation was mainly extracted from Fahy's and Lindqvist's work. Here, the word "analytical" groups many things. The rib dynamics was represented by classical wave propagation models and restricted to Euler flexural waves and torsional waves. Plate bending was modeled by using Kirchhoff–

Love equations. The analytical respect of coupling between ribs and plate leads to the analytical estimation of "coupled" wavenumbers. The resulting analytical developments lead to an "unwieldy" derivation so that analytical estimation strategies are only feasible for simple configurations.

- The wave motion of homogeneous and periodic slender structures was studied, with emphasis being given to the extraction of guided elastic wave properties by finite elements. A numerical procedure was provided in order to extract the propagation parameters of any thin walled structure. The dispersion curves of a complex guided structures were shown over a wide frequency range. The procedure was also implemented in a finite element code, leading to an effective tool for analyzing free waves in realistic situations. Furthermore, a spectral problem relating to propagation behavior was established in a finite element schema. The solution of this spectral problem at each frequency step defined all the requisite properties. The eigenvalues were related to guided wavenumbers and the eigenvectors defined the guided wave mode shapes. The evolution of the frequency of the guided wavenumbers/mode shapes revealed relative complexity.
- A numerical experiment was proposed here in the case of rib-stiffened plates. Comparisons with analytical wave propagation estimations over a wide frequency range showed very good agreement. What is more the numerical method provided is very easy to use and has general and generic advantages.
- Comparisons of the $(k_{x'}(\omega))$ dispersion curves obtained experimentally with the numerical implemented method were also provided. The *multi-mode wave propagation process* in the rib-stiffened plate described in the companion paper was clearly shown here and the numerical/experimental results agree well.

Further investigations relating to the results presented in this contribution are in progress. Extending the IWC method is an important issue of this work and further applications of this method to complex structures (sandwich honeycomb built-up structures, different ribbed panels, etc.) are in progress and will provide insights into their behavior up to high frequencies.

References

Benerjee, S., Kundu, T., 2006a. Elastic wave propagation in sinusoidally corrugated waveguides. Journal of Acoustical Society of America 119 (4), 2006–2017.

Benerjee, S., Kundu, T., 2006b. Symmetric and anti-symmetric rayleigh-lamb modes in sinusoidally corrugated waveguides. International Journal of Solids and Structures 43 (21), 6551–6567.

Bocquillet, A., Ichchou, M.N., Jezequel, L., 2003. Energetics of axisymmetric fluid-filled pipes up to high frequencies. Journal of Fluids and Structures 17, 491–510.

Broullouin, L., 1953. Wave Propagation in Periodic Structures. Dover Publication.

Cordonnier-Cloarec, P., 1989. Contribution a l'Ttude du rayonnement acoustique de parois mTtalliques nervurTes. Ph.D. Thesis.

Fahy, F.J., Lindqvist, E., 1976. Wave propagation in damped, stiffened structures characteristic of ship construction. Journal of Sound and Vibration 45 (1), 115–138.

Finnveden, S., 1994. Exact spectral finite element analysis of stationary vibrations in a railway car structure. Acta Acoustica (2), 433–449.

Finnveden, S., 1997. Spectral finite element analysis of the vibration of straight fluid-filled pipes with flanges. Journal of Sound and Vibration 199 (1), 125–154.

Gavric, L., 1994. Finite element computation of dispersion properties of thin walled waveguides. Journal of Sound and Vibration 173 (1), 113–124.

Houillon, L., Ichchou, M.N., Jezequel, L., 2005. Wave motion in thin walled structures. Journal of Sound and Vibration 281 (3–5), 483–507.

Ichchou, M.N., Berthaut, J., Collet, M., accepted for publication. Multi-mode wave propagation ribbed plates: Part I, k-space characteristics. International Journal of Solids and Structures 45(5), 1179–1195.

Knothe, K., Strzyzakowsk, Z., Wilner, K., 1994. Rail vibrations in the high frequency range. Journal of Sound and Vibration 169 (1), 111–123.

Lin, Y.K., Donaldson, B.K., 1969. A brief survey of transfer matrix techniques with special reference to the analysis of aircraft panels. Journal of Sound and Vibration 10 (1), 103–143.

Mace, B., Duhamel, D., Brennan, M.J., Hinke, L., 2005. Finite element prediction of wave motion in structural waveguides. Journal of Acoustical Society of America 2005 (117), 2835.

Mead, D.J., 1973. A general theory of harmonic wave propagation in linear periodic systems with multiple coupling. Journal of Sound and Vibration 27 (2), 235–260.

Mead, D.J., 1975. Wave propagation and natural modes in periodic systems: multi-coupled systems, with and without damping. Journal of Sound and Vibration 40 (1), 19–39.

Mencik, J.-M., Ichchou, M.N., 2005. Multi-mode propagation and diffusion in structures through finite elements. European Journal of Mechanics-A/Solids 24 (5), 877–898.

Mencik, J.-M., Ichchou, M.N., 2007. Wave finite elements in guided elastodynamics with internal fluid. International Journal of Solids and Structures (7-8), 2148–2167.

Orrenius, U., Finnveden, S., 1996. Calculation of wave propagation in rib-stiffened plate structures. Journal of Sound and Vibration 198 (2), 203–224.

Timoshenko, S., 1921. On the correction of transverse shear deformation of the differential equations for transverse vibrations of prismatic bars. Philosophical Magazine 6 (41).

Timoshenko, S.P., Woinowski-Krieger, S., 1989. Theory of Plates and Shells, seconnd ed. McGraw-Hill International Editions, New York.

Tompson, D.J., 1993. Wheel-rail noise generation, part IV: contact zone and results. Journal of Sound and Vibration 161 (3), 447–466.

Yong, Y., Lin, Y.K., 1989. Propagation of decaying waves in periodic and piecewise periodic structures of finite length. Journal of Fluids and Structures (2), 99–118.

Zhong, W.X., Williams, F.W., 1995. On the direct solution of wave propagation for repetitive structures. Journal of Sound and Vibration 181 (3), 485–501.